Hindawi
Adsorption Science & Technology
Volume 2022, Article ID 4273900, 19 pages
https://doi.org/10.1155/2022/4273900

Research Article

Fractal Pore and Its Impact on Gas Adsorption Capacity of Outburst Coal: Geological Significance to Coalbed Gas Occurrence and Outburst

Guangjun Feng,[1,2] **Xinzhuo Zhao**,[3] **Meng Wang**,[1,4] **Yu Song**,[1,2] **Sijian Zheng**,[4] **Ye He**,[5] **and Zhenjiang You**[6,7]

[1]*Key Laboratory of Coalbed Methane Resources and Reservoir Formation Process, Ministry of Education, China University of Mining and Technology, Xuzhou 221008, China*
[2]*School of Resources and Geosciences, China University of Mining and Technology, Xuzhou 221116, China*
[3]*No.5 Exploration Institute of Geology and Mineral Resources of Shandong Province, Taian 271000, China*
[4]*Carbon Neutrality Institute, China University of Mining and Technology, Xuzhou 221008, China*
[5]*Xuzhou Coal Mining Group Co., Ltd., Xuzhou 221018, China*
[6]*Center for Sustainable Energy and Resources, Edith Cowan University, Joondalup, WA 6027, Australia*
[7]*School of Chemical Engineering, The University of Queensland, Brisbane, QLD 4072, Australia*

Correspondence should be addressed to Xinzhuo Zhao; 13581190323@163.com and Meng Wang; wangm@cumt.edu.cn

Received 15 May 2022; Revised 3 September 2022; Accepted 14 October 2022; Published 9 November 2022

Academic Editor: Senthil Kumar Ponnusamy

Pore structure and methane adsorption of coal reservoir are closely correlated to the coalbed gas occurrence and outburst. Full-scale pore structure and its fractal heterogeneity of coal samples were quantitatively characterized using low-pressure N_2 gas adsorption (LP-N_2GA) and high-pressure mercury intrusion porosimetry (HP-MIP). Fractal pore structure and adsorption capacities between outburst and nonoutburst coals were compared, and their geological significance to gas occurrence and outburst was discussed. The results show that pore volume (PV) is mainly contributed by macropores (>1000 nm) and mesopores (100–1000 nm), while specific surface area (SSA) is dominated by micropores (<10 nm) and transition pores (10–100 nm). On average, the PV and SSA of outburst coal samples are 4.56 times and 5.77 times those of nonoutburst coal samples, respectively, which provide sufficient place for gas adsorption and storage. The pore shape is dominated by semiclosed pores in the nonoutburst coal, whereas open pores and inkbottle pores are prevailing in the outburst coal. The pore size is widely distributed in the outburst coal, in which not only micropores are dominant, but also, transition pores and mesopores are developed to a certain extent. Based on the data from HP-MIP and LP-N_2GA, pore spatial structure and surface are of fractal characteristics with fractal dimensions D_{m1} (2.81–2.97) and D_n (2.50–2.73) calculated by Menger model and Frenkel–Halsey–Hill (FHH) model, respectively. The pore structure in the outburst coal is more heterogeneous as its D_n and D_{m1} are generally larger than those of the nonoutburst coal. The maximum methane adsorption capacities (V_L: 15.34–20.86 cm^3/g) of the outburst coal are larger than those of the nonoutburst coal (V_L: 9.97–13.51cm^3/g). The adsorptivity of coal samples is governed by the micropores, transition pores, and D_n because they are positively correlated with the SSA. The outburst coal belongs to tectonically deformed coal (TDC) characterized by weak strength, rich microporosity, complex pore structure, strong adsorption capacity, but poor pore connectivity because of inkbottle pores. Therefore, the area of TDC is at high risk for gas outburst as there is a high-pressure gas sealing zone with abundant gas enrichment but limited gas migration and extraction.

1. Introduction

Coalbed methane is a serious safety hazard in coal mines [1, 2], while it is also an important economical natural gas supply [3, 4]. The mechanism of gas occurrence, emission, and outburst is not only controlled by macroscopic geological factors [5, 6] but also closely correlated to the microscopic structure in coal reservoirs [7, 8]. The effects of geological factors on gas occurrence and outburst have been studied extensively [9–11]. However, it is still necessary to further study geological significance from the perspective of porosity and adsorptivity in coal reservoirs. The solid-gas coupling between coal and methane is essentially the interaction between gas and inner pores [12], and pore structure directly influences the occurrence of adsorbed gas and free gas in coal seams [13–19]. Therefore, the investigation into pore structure and methane adsorption capacity of coal is the key to analyzing the microscopic mechanism of coalbed gas occurrence and outburst, which is critical to safety mining and coalbed methane resource evaluation.

Coal is a type of porous medium, in which the well-developed pore network provides the storage place and seepage channel for gas [20–24]. The decimal classification is widely adopted in coal pore research [25], namely, micropores (<10 nm), transition pores (10–100 nm), mesopores (100–1000 nm), and macropores (>1000 nm). Generally, pore structure in coal reservoirs can be characterized by image analysis [18, 26], fluid intrusion [27, 28], gas adsorption [13, 15, 29], small-angle scattering of X-rays (SAXS), and neutrons (SANS) [30, 31]. Among them, high-pressure mercury intrusion porosimetry (HP-MIP) has been commonly used in pore characterization for obtaining quantitative information in a wide pore size range (3 nm–100 μm) [28, 32]. It should be pointed out that the mercury intrusion pressure is extremely high in determining nanopores. For example, the maximum intrusion pressure can reach 413.7 MPa, which corresponds to a pore size of 3 nm. The high-pressure mercury may destroy the original pore structure. Furthermore, the compression effect on coal matrix intensifies at high pressures [13, 33]. Consequently, HP-MIP is recommended for the characterization of pores with a diameter above 50 nm because of the practical errors in characterizing pores with smaller sizes [8, 14]. However, low-pressure N_2 gas adsorption (LP-N_2GA) can accurately measure nanopores in coal reservoirs, which overcomes the limitation of HP-MIP. Therefore, the advantages of HP-MIP and LP-N_2GA should be combined to achieve the full-scale pore characterization in coal samples and obtain accurate details, such as specific surface area (SSA), pore volume (PV), pore size distribution (PSD), pore shape, pore openness, and connectivity.

Due to the complexity of the pore network in coal, the heterogeneity of pore structure is difficult to be described in light of the traditional Euclidean geometry theory, while with the application of modern fractal theory, fractal dimension can quantitatively characterize the complexity of pore structure [16, 34]. Adopting Frenkel-Halsey-Hill (FHH) and Menger models to analyze the data from LP-N_2GA and HP-MIP, Yao et al. [15, 28] described the fractal characteristics of nanoscale pores (<100 nm) and micron-scale pores (>100 nm) for different-rank coal, respectively. The fractal heterogeneity of coal pores leads to differences in SSA and gas adsorption capacity [35]; thus, it is necessary to perform a comparative study on fractal pore characteristics between outburst and nonoutburst coals.

Methane is mainly stored in coal as patterns of adsorbed gas, free gas, and dissolved gas [36]. Adsorbed gas accounts for 80%–90% of the total gas content in coal reservoirs [14, 37]. The methane adsorptivity of coal is vital to gas content and gas pressure. Usually, adsorption isotherms are obtained from methane adsorption experiments in the laboratory [20, 38], and adsorption parameters are calculated by fitting an appropriate adsorption model to quantify the adsorption capacities of coal samples. The gas adsorption capacities for coal reservoirs are not only affected by external conditions such as pressure, temperature, and moisture content [39, 40] but also closely related to coal properties including coal rank, maceral composition, pore parameters, and fractal dimension [16, 41, 42]. Tectonically deformed coal (TDC) is prevalent in China, which is usually associated with coal and gas outburst [12, 43]. The coal strength, pore structure, and fractal heterogeneity all changed significantly from the native structure (primary coal) to TDC [12, 43, 44]. However, the pore structure and fractal heterogeneity caused by tectonic deformation and their influence on gas adsorption and occurrence still need to be further studied.

This study focuses on the fractal pore and gas adsorption capacity of the outburst coal and their geological significance to coalbed gas occurrence and outburst. HP-MIP and LP-N_2GA were performed to jointly characterize the full-scale pore structure in coal samples. According to the branches of mercury intrusion and nitrogen adsorption, the fractal dimensions were calculated to study the fractal heterogeneity of microscopic pore structure. Isothermal adsorption experiments were performed to determine methane adsorption capacities of coal samples and discover the effects of pore structure and fractal dimension on gas adsorptivity. Moreover, we compared the difference of fractal pores and adsorbability between the outburst coal and nonoutburst coal and revealed their geological significance to gas occurrence and outburst. This study helps to understand coalbed gas geological occurrence and prevent coal and gas outburst.

2. Samples and Methodology

2.1. Geological Background and Sampling. The study area is located in the Qianjiaying coal mine, Kaiping coalfield, China (Figure 1(a)). Main coal seams are distributed in the Upper Carboniferous to Lower Permian Damiaozhuang Formation, and the study area is structurally located in the southeastern Kaiping syncline (Figure 1(b)). The burial depth of coal seam increases from southeast to northwest. The content and pressure of coalbed gas are generally consistent with the variation trend of burial depth, as well as gas occurrence closely controlled by folds and faults. There are two high-risk areas of coal and gas outburst delineated based on gas content, gas pressure, structural complexity,

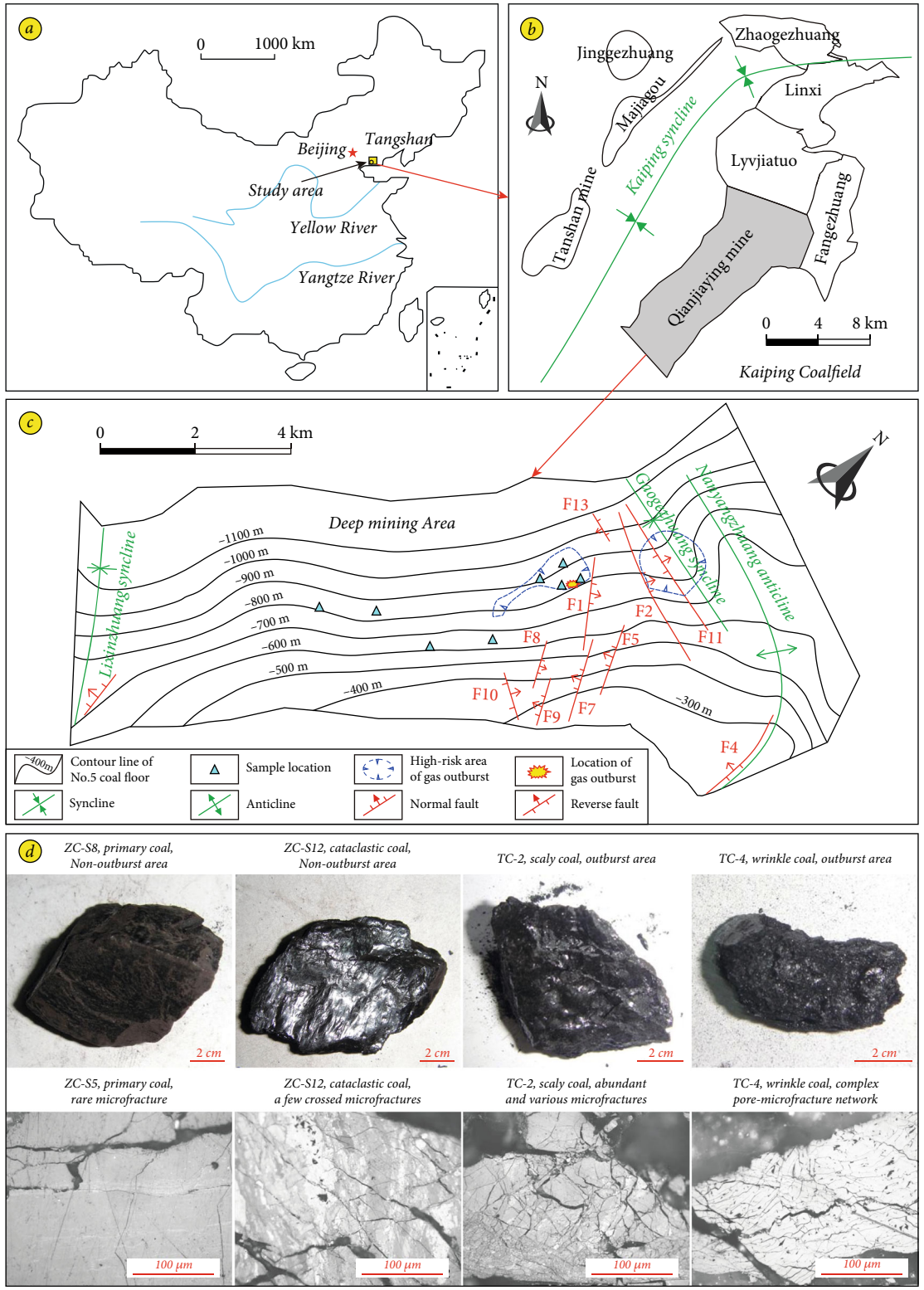

Figure 1: Location of the study area (a, b), structural outline map of the coal mine (c), and macroscopic and microscopic characteristics of the coal samples (d).

and variation coefficient of coal thickness, comprehensively. The study area had experienced a gas anomaly and outburst, with a volume of 7380 m^3 gas emission and 489 t of pulverized coal and rock block ejection at the main crosscut on the -850 m level (Figure 1(c)), which provides a good comparative object for the present study.

Eight coal samples were collected from the gas anomaly and outburst area and nonoutburst area (Table 1). The coal

Table 1: Basic information and testing data of the coal samples.

Sample ID	Sampling location	Tectonically deformed types	$R_{o,max}$	Proximate analysis (%)			
				M_{ad}	A_{ad}	V_{daf}	FC_{ad}
ZC-S5	Nonoutburst area	Primary coal	1.32	2.02	22.7	23.44	51.84
ZC-S8		Primary coal	1.29	1.13	20.83	24.75	53.29
ZC-Q9		Cataclastic coal	1.49	1.10	21.12	29.96	47.82
ZC-S12		Cataclastic coal	1.55	1.43	21.16	27.81	49.60
TC-1	Gas anomaly and outburst area	Scaly coal	1.33	0.35	15.79	28.27	55.59
TC-2		Scaly coal	n/a	0.44	23.51	26.49	49.56
TC-3		Wrinkle coal	1.58	1.08	23.25	28.15	47.52
TC-4		Wrinkle coal	n/a	0.87	18.84	31.33	48.96

Notes: n/a: no available data; M_{ad}: moisture content, air dry basis; A_{ad}: ash content, air dry basis; V_{daf}: volatile content, air dry basis; FC_{ad}: fixed carbon, air dry basis.

samples from gas anomaly and outburst areas mainly belong to scaly coal and wrinkle coal because of the tectonic deformation and coal seam rheology, whereas the samples from nonoutburst areas are mainly primary coal and cataclastic coal (Figure 1(d)). Compared with the primary coal, TDC in the outburst area is characterized by low strength, low firmness, and poor stability through the observation on sample specimen. According to microscopic observation, there are rare microfractures and a few crossed microfractures in primary coal and cataclastic coal, respectively. However, abundant and various microfractures formed a complex network connecting pores in the scaly coal and wrinkle coal from the gas outburst area (Figure 1(d)). The coal samples belong to coking coal with measured vitrinite reflectance ($R_{o,max}$) ranging within 1.29%–1.58% (Table 1). According to the proximate analysis, all the coal samples are characterized by low moisture content, as well as high ash and volatile content. Coal rank and coal quality have significant effects on gas adsorption. Due to the small-scale alteration for the above two properties among the samples, we focus on the effect of fractal pore structure on methane adsorption capacities of the coal samples.

2.2. Experimental Methods

2.2.1. High-Pressure Mercury Intrusion Porosimetry. HP-MIP experiments were conducted using an AutoPore 9510 mercury porosimeter (Micrometrics Instrument, USA) at the Key Laboratory of Coalbed Methane Resources and Reservoir Formation Process, China University of Mining and Technology. According to the China National Standard GB/T 21650.1-2008, coal samples were broken down to about 2×2 mm. Then, 3–5 g granular sample was oven-dried at 110°C for 12 h to remove moisture and impurity gas. Afterwards, the instrument was vacuumized before testing and loaded with the dry samples for the experiment. Mercury was injected into the coal samples with the pressure range from 690 Pa to 413.7 MPa, corresponding to the lower limits of detected pore size 3 nm. Owing to the effect of the surface tension, the relationship between the pressure of intrusion mercury and pore size can be expressed by the Washburn equation [45]. The amount of intrusion and extrusion mercury at different pressures was recorded to calculate the parameters of pore structure. Meanwhile, the results with pore size greater than 100 μm should be removed, which are considered to be interfered by particle accumulation or surface cracks.

2.2.2. Low-Pressure N_2 Gas Adsorption. LP-N_2GA measurements were carried out at the Key Laboratory of Coal Preparation & Purification, China University of Mining and Technology, using a specific surface and pore size analyzer (Autosorb IQ, Quantachrome, USA), which can detect the pore size ranging within 0.35–200 nm. The resolution of the microporous test can reach 0.02 nm, and the minimum detectable SSA and PV are 0.0005 m^2/g and 0.0001 cm^3/g, respectively. Based on the China National Standard GB/T19587-2004, the coal samples were crushed into 0.18–0.25 mm (60–80 mesh). Then, 5–8 g coal powder samples were dried at 110°C for 12 h in an oven to remove impurity fluids including water vapor. After sample drying, all coal powders were evacuated for complete outgassing in a high vacuum system within 5 h. Using N_2 gas with a purity of 99.99%, adsorption and desorption isotherms of coal powders were measured successively with the relative pressures (P/P_0: 0.009–0.998) at the temperature of 77.4 K. According to the N_2 adsorption branch, the multipoint Brunauer-Emmett-Teller (BET) model and Barrett-Joyner-Halenda (BJH) model [46–48] were chosen to calculate the SSA and PV, respectively. The PSDs were derived based on the density functional theory (DFT) model [49, 50].

2.2.3. Methane Adsorption Experiment. Isothermal adsorption experiments were carried out adopting an IS-300 volumetric adsorption and desorption analyzer (TerraTek, USA) at the Key Laboratory of Coalbed Methane Resources and Reservoir Formation Process, China University of Mining and Technology. Firstly, the coal samples were crushed into 0.18–0.25 mm (60–80 mesh). Secondly, 120–150 g pulverized coal powder was prepared as the equilibrium water sample at the relative humidity of 98%. Lastly, using the pure methane gas (purity: 99.99%), adsorption measurements were performed with pressures ranging within 0–8 MPa at a constant temperature (30°C). The pressure data of both

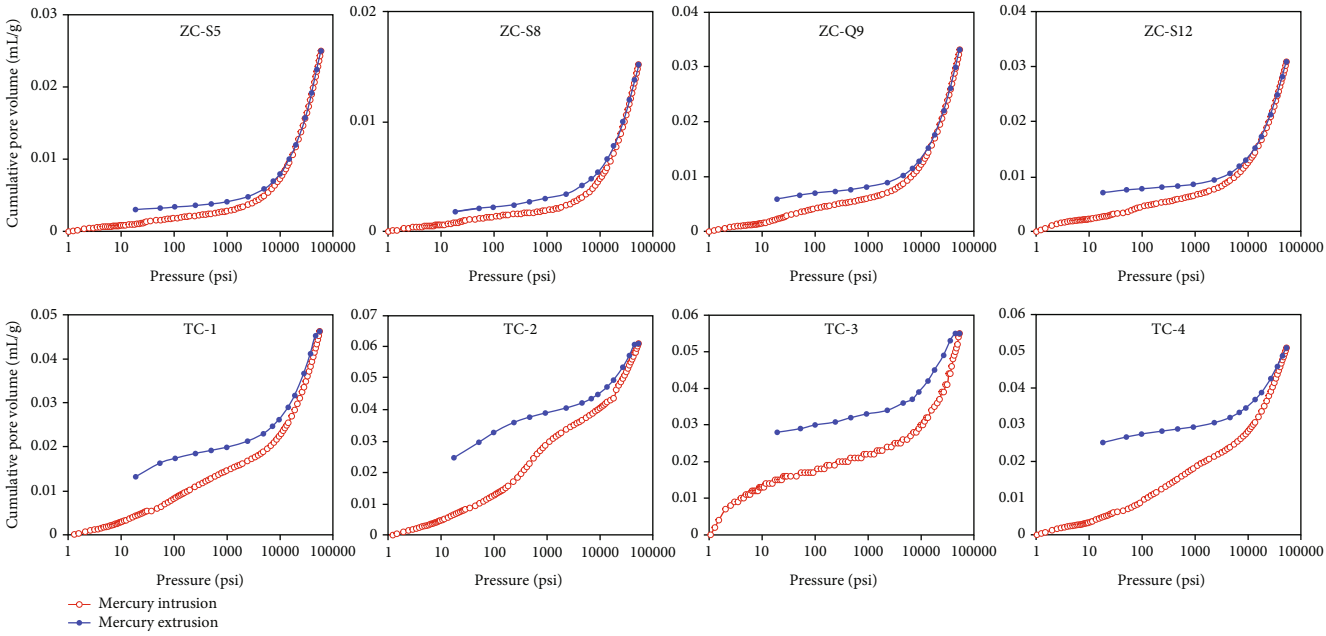

Figure 2: Mercury intrusion and extrusion curves of the coal samples.

the sample cell and reference cell was recorded to calculate the adsorbed methane content of the coal samples. The Langmuir model (Equation (1)) [51] was chosen to fit the adsorption data and further determine the relevant parameters and isotherms for the coal samples:

$$V = \frac{PV_L}{P + P_L}, \tag{1}$$

where P is testing pressure, MPa; V is methane adsorption content at the pressure P, cm^3/g; V_L is the Langmuir volume, which reflects the maximum methane adsorption capacity, cm^3/g; and P_L is the Langmuir pressure, MPa.

2.3. Fractal Dimension Analysis. Based on the fractal theory, the heterogeneity and complexity of pore structure can be quantitatively evaluated with fractal dimension. In this study, the fractal dimensions with different pore size ranges were determined based on the HP-MIP and LP-N_2GA data, denoted as D_m and D_n, respectively. The Menger sponge model was applied to D_m calculation [28], which is expressed as

$$\ln\left(\frac{dV_p}{dP}\right) \propto (D_m - 4)\ln P, \tag{2}$$

where D_m is the fractal dimension calculated from HP-MIP data, dimensionless; P is the intrusion mercury pressure, MPa; and V_p is the cumulative mercury volume at the pressure P, mL/g.

As long as the fractal characteristics exist in the pore structure, $\ln(dV_p/dP)$ and $\ln P$ exhibit a linear correlation. Furthermore, the slope K_m of the linear correlation can be obtained to calculate the fractal dimension D_m.

The Frenkel-Halsey-Hill (FHH) model was widely adopted for fractal dimension determination, which is shown in the following equation:

$$\ln(V) = (D_n - 3)\cdot \ln\left[\ln\left(\frac{P_0}{P}\right)\right] + C, \tag{3}$$

where D_n is the fractal dimension calculated from LP-N_2GA data, dimensionless; C is a constant dimensionless; P/P_0 is relative pressure, dimensionless; and V is the adsorbed gas volume at P/P_0, cm^3/g.

If the pore structure is characterized by fractal heterogeneity, $\ln V$ exhibits a linear correlation with $\ln[\ln(P_0/P)]$. Solving the slope K_n of the linear correlation, the fractal dimension D_n can be further calculated, and the fractal dimension is generally divided into two stages (D_{n1} and D_{n2}). It should be noted that both the D_m and D_n values should be between 2 and 3 [52, 53], and a larger fractal dimension indicates a stronger fractal heterogeneity of pore structure.

3. Results

3.1. Pore Characterization Using HP-MIP. The mercury intrusion and extrusion curves are illustrated in Figure 2 for all the coal samples. For the nonoutburst coal samples, the amount of mercury intrusion increased slowly at the low pressures but increased rapidly while pressure is over 5000 psi, indicating that micropores are relatively rich compared to larger-size pores. Both mercury intrusion branch and extrusion branch are concave-up curves, and hysteresis loops are narrow for nonoutburst coal samples. It is speculated that semiclosed pores are dominant in the nonoutburst coal samples, resulting in poor openness and connectivity. For the outburst coal samples, the amount of mercury

intrusion increases consistently with pressure from the initial stage to the high-pressure stage, indicating that the PSDs are relatively uniform in the samples. With the decrease of pressure, the mercury extrusion curves initially decreased rapidly, then tended to be flat (sample TC-3 and TC-4), and finally presented a sharp decline with the upper convex shape (sample TC-1 and TC-2). The hysteresis loops are relatively wide for outburst coal samples as a result of the considerable difference in the volume between mercury intrusion and extrusion. Hence, the outburst coal mainly contains open pores, but the inkbottle pores with narrow throats occupy a substantial proportion, which leads to poor pore connectivity.

The parameters of pore structure obtained from HP-MIP are shown in Table 2. The measured porosity of coal samples varies between 2.24% and 7.29%. The PV of macropores and mesopores range within 0.0012–0.0174 cm^3/g and 0.0006–0.0170 cm^3/g, respectively. And the SSAs of macropores and mesopores are 0.001–0.015 m^2/g and 0.012–0.249 m^2/g, respectively. The relationship between incremental intrusion volume and pore size is plotted in Figure 3. The PSDs are unimodal for the nonoutburst coal samples (Figure 3(a)), and incremental intrusion volume possesses a peak at the range of micro- and transition pores. However, the PSDs are relatively uniform for the outburst coal samples (Figure 3(b)), showing a multimodal distribution, and two major peaks appear in micropores and mesopores. It should be noted that HP-MIP has advantages in macro- and mesopore characterization, though the accuracy is questionable in characterizing pores with a diameter below 50 nm. So the PSDs of pores (<50 nm) should be further analyzed in combination with LP-N_2GA.

3.2. Pore Characterization Using LP-N_2GA. LP-N_2GA results show that N_2 adsorption curves are in reverse "S" shape for all the coal samples (Figure 4). The shape of adsorption curves depends on the interaction between nitrogen and pore surface in different pressure ranges [54]. When $P/P_0 < 0.01$, the adsorption branches rise sharply because of micropore filling, indicating well-developed micropores in the coal samples. Then, the adsorption curves present a knee-bend shape at the stage of $0.01 < P/P_0 < 0.05$, which indicates the monolayer adsorption process of nitrogen molecules covering the entire pore surface based on the technical report proposed by the International Union of Pure and Applied Chemistry (IUPAC) [48, 54]. Subsequently, the adsorbed volume increases slowly as a result of the transition from monolayer adsorption to multilayer adsorption. Finally, at high relative pressures ($P/P_0 > 0.9$), the adsorption curves rise remarkably and fail to reach adsorption saturation even if P/P_0 approaches 1.0, indicating the capillary condensation occurs in pores. There are hysteresis loops between adsorption and desorption branches (Figure 4) because of the capillary condensation. The hysteresis loops are relatively narrow for nonoutburst coal samples as their adsorption curves almost overlap with desorption curves. In the light of the hysteresis loop classification recommended by IUPAC [54], the hysteresis loops of the nonoutburst coal are similar to the type H4 hysteresis loop, implying that the narrow slit-like pores, wedge pores, and conical pores are prevailing in the nonoutburst coal. However, the hysteresis loops of the outburst coal possess larger width and appear to have a sharp decline at the P/P_0 of 0.5, which are similar to type H2(b) based on the classification, as well as present the characteristics of type H3 hysteresis loop at high pressures. Therefore, there are plate-shaped pores, cylindrical pores with open ends, and inkbottle pores with a wide body but a narrow throat in the outburst coal samples.

According to the results measured by LP-N_2GA (Table 2), the PV of micro- and transition pores in the coal samples are 0.0001–0.0022 cm^3/g and 0.0005–0.0036 cm^3/g, respectively. The SSAs of micro- and transition pores are 0.052–2.706 m^2/g and 0.074–0.602 m^2/g, respectively. LP-N_2GA has an advantage in the characterization of PSDs of the micro- to transition pores. According to the PSDs calculated using the DFT model presented in Figure 5, the PSDs of the nonoutburst coal samples show multimodal with the peaks in the pore size ranges of 18–20 nm, 30–50 nm, and 70–80 nm (Figure 5(a)). Although the multimodal feature of the PSDs is apparent for the outburst coal samples (Figure 5(b)), the peaks are distributed over a relatively wide pore size range (3–80 nm).

3.3. Pore Fractal Heterogeneity of the Coal Samples. Based on the data from mercury intrusion branches of the coal samples, the correlations between $\ln(dV_p/dP)$ and $\ln P$ are plotted in Figure 6. Two different linear correlations are shown at pressure ranges of 0.01–24 MPa and 24–413.7 MPa, and the pore size at the transition point between the two linear correlations is approximately 50 nm. When the pore diameter is over 50 nm ($D > 50$ nm), there is a strong linear relationship between $\ln(dV_p/dP)$ and $\ln P$ with the coefficient of determination (R^2) above 0.96 for all the coal samples (Table 3). Furthermore, the fractal dimension D_{m1} was calculated according to the Menger model (Equation (2)), which ranges from 2.81 to 2.97. The values of D_{m1} are close to the upper limit 3, indicating that the pore structure ($D > 50$ nm) is relatively complex in the coal samples. Nevertheless, for the pore diameter of 3–50 nm, the correlations between $\ln(dV_p/dP)$ and $\ln P$ are relatively weak, especially for sample ZC-S8 ($R^2 = 0.3823$) and sample TC-2 ($R^2 = 0.4517$). In addition, the calculated fractal dimension values D_{m2} range from 3.63 to 3.83, which all exceed the upper limit 3 and become invalid. The previous studies have shown that the compressibility of coal presents a remarkable impact on the HP-MIP data when mercury intrusion pressure is beyond 20 MPa [13, 16]. For HP-MIP measurements at high pressures, the mercury intrusion volume per unit pressure is larger than the actual pore volume because of matrix compression in the coal samples, resulting in errors in D_{m2} calculation for the pores below 50 nm. Thus, our results also confirmed that HP-MIP is inadequate in the characterization of pores below 50 nm.

To overcome the limit of fractal dimension calculation in pores ranging within 3–50 nm from HP-MIP data, the fractal dimension D_n of pores ranging within 1–50 nm was

Table 2: Pore structure parameters of the coal samples measured by HP-MIP and LP-N_2GA.

Sample	Porosity (%)	Pore volume (cm^3/g)				Specific surface area (m^2/g)				Total PV (cm^3/g)	Total SSA (m^2/g)
		Macropores HP-MIP	Mesopores HP-MIP	Transition pores LP-N_2GA BJH	Micropores LP-N_2GA BJH	Macropores HP-MIP	Mesopores HP-MIP	Transition pores LP-N_2GA BET	Micropores LP-N_2GA BET		
ZC-S5	3.06	0.0017	0.0013	0.0008	0.0002	0.002	0.023	0.130	0.266	0.0041	0.421
ZC-S8	2.24	0.0012	0.0006	0.0005	0.0001	0.001	0.012	0.074	0.052	0.0024	0.139
ZC-Q9	3.92	0.0040	0.0020	0.0010	0.0004	0.006	0.034	0.164	0.435	0.0074	0.640
ZC-S12	3.98	0.0039	0.0022	0.0012	0.0005	0.004	0.037	0.182	0.389	0.0078	0.612
TC-1	5.31	0.0092	0.0060	0.0023	0.0014	0.010	0.088	0.381	1.578	0.0188	2.057
TC-2	7.29	0.0140	0.0170	0.0036	0.0014	0.011	0.249	0.602	1.837	0.0360	2.699
TC-3	4.69	0.0174	0.0040	0.0028	0.0013	0.015	0.061	0.444	1.868	0.0255	2.388
TC-4	6.79	0.0089	0.0071	0.0027	0.0022	0.007	0.137	0.444	2.706	0.0208	3.294

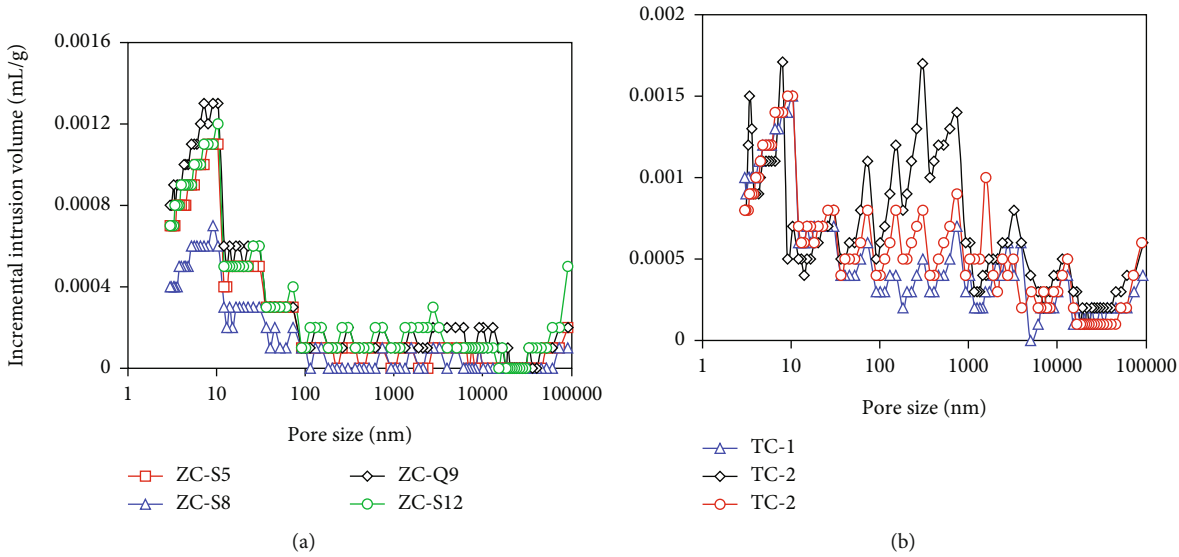

Figure 3: Relationship between incremental intrusion volume and pore size for nonoutburst coal samples (a) and outburst coal samples (b).

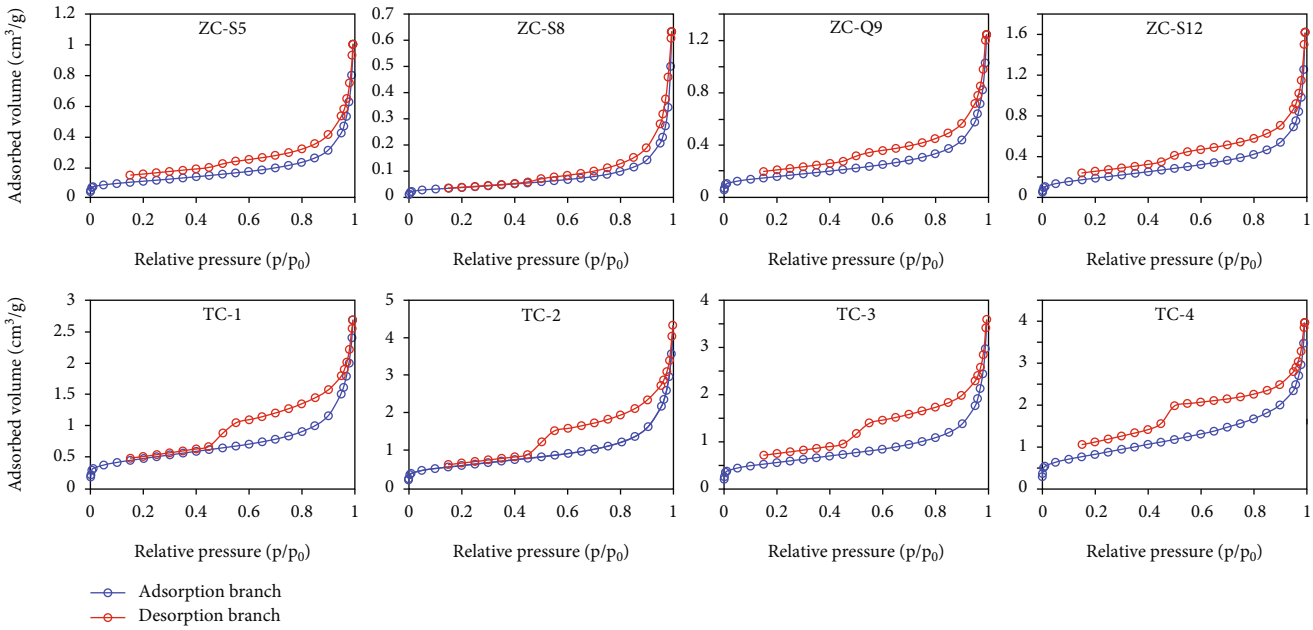

Figure 4: N_2 adsorption and desorption isotherms of the coal samples.

calculated based on N_2 adsorption branches (Table 3). As exhibited in Figure 7, the correlations between ln V and ln [ln (P_0/P)] are linear with R^2 above 0.98 for all the coal samples. According to the FHH model (Equation (3)), the fractal dimension D_n was calculated with the value of 2.50–2.73. Comparatively, the D_n is smaller than D_{m1}, which reflects that the heterogeneity of pores above 50 nm is stronger than that of pores ranging within 1–50 nm.

3.4. Adsorption Isotherms of the Coal Samples. As illustrated in Figure 8 and Table 4, the methane adsorption capacities of all the coal samples were determined through methane adsorption experiments on the equilibrium water samples at 30°C. The adsorption isotherms were well fitted adopting the Langmuir model (Equation (1)), with R^2 above 0.99 for all the coal samples, and the adsorption parameters were further obtained. The Langmuir volume (V_L) of coal samples ranges from 9.97 cm^3/g to 20.86 cm^3/g, and the Langmuir pressure (P_L) ranges from 0.93 MPa to 1.42 MPa (Table 4). Obviously, the V_L of the outburst coal samples (15.34–20.86 cm^3/g) is larger than that of the nonoutburst coal samples (9.97–13.51 cm^3/g), which indicates that the outburst coal possesses stronger methane adsorption capacities.

4. Discussion

4.1. Effect of Pore Structure on Methane Adsorption Capacity. The adsorption capacity of coal is an important factor

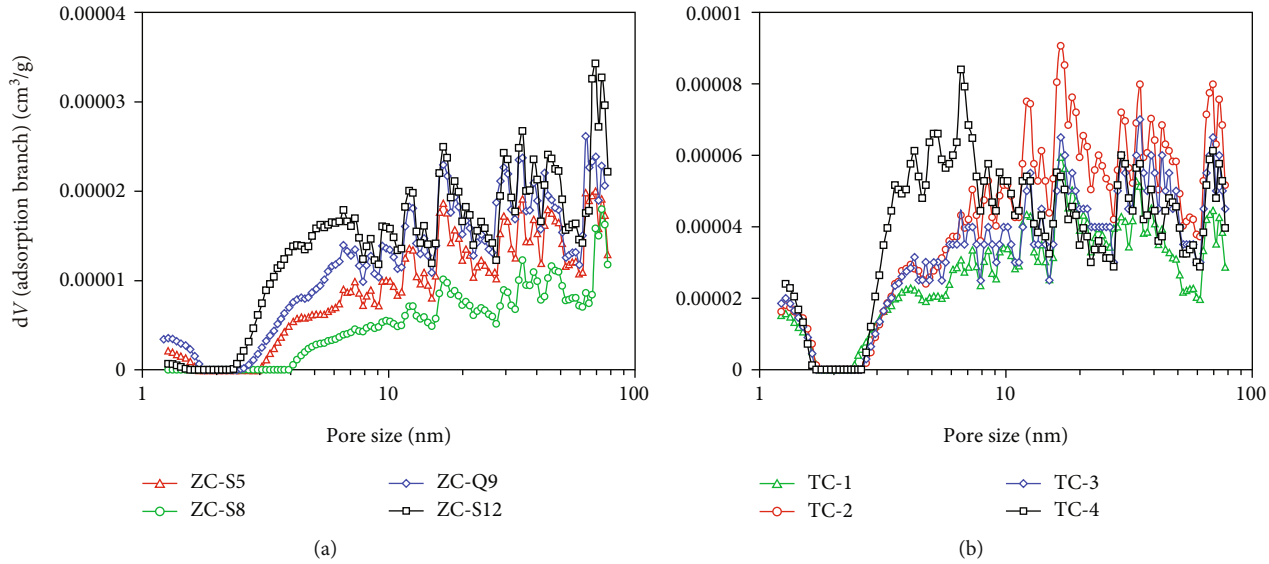

FIGURE 5: Relationship between incremental adsorbed volume and pore size for nonoutburst coal samples (a) and outburst coal samples (b).

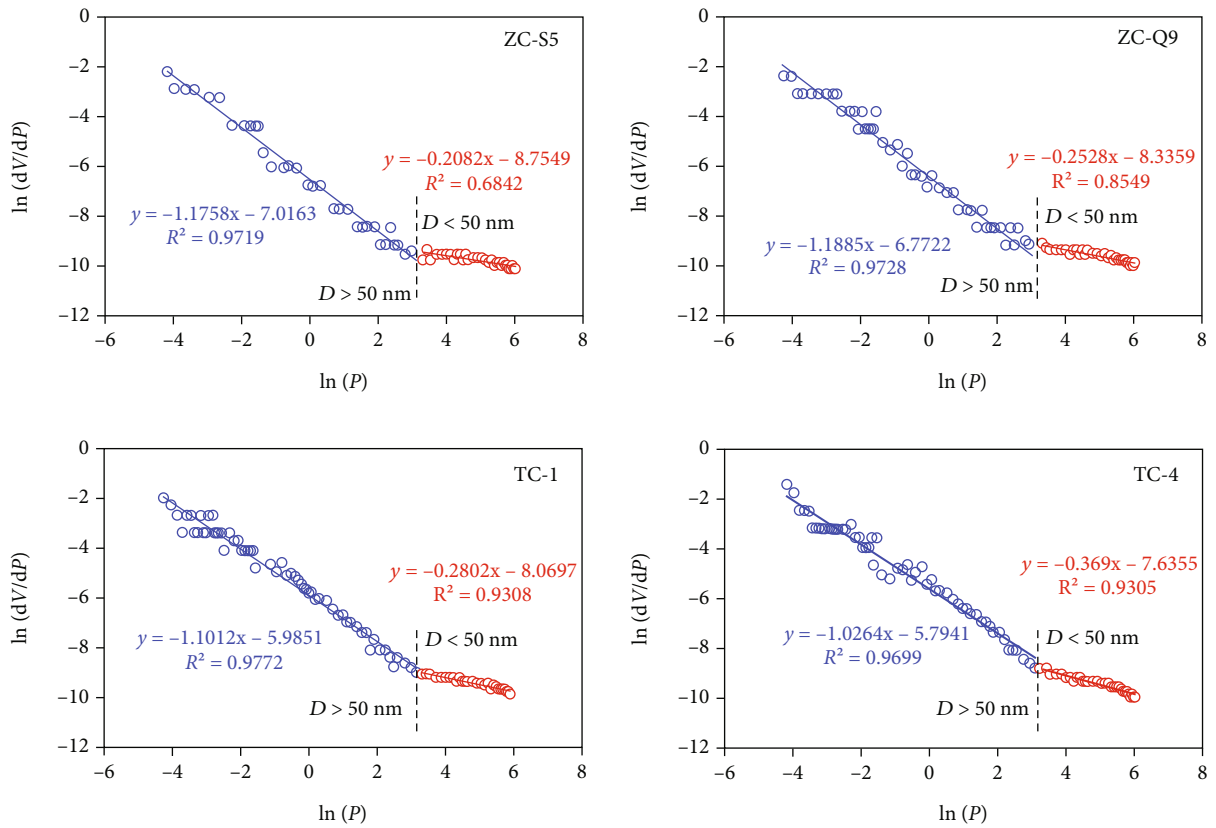

FIGURE 6: Plots of ln (dV/dP) and ln (P) of the representative coal samples based on the HP-MIP measurements.

affecting the gas content in the coal mine. As the place where gas interacts with coal matrix, the pore properties are the most direct factor affecting the methane adsorption in coal reservoir. Also, coal rank, maceral, and other factors can indirectly affect the adsorption performance of coal by controlling the pore structure [13, 41]. According to the scatter diagrams of total PV and SSA versus the maximum methane adsorption capacities of the coal samples (Figure 9), there is a strong positive correlation between V_L and SSA (R^2 = 0.9410). The maximum methane adsorption capacities increase with the increase of the SSA (Figure 9(b)). Therefore, the adsorptivity of the coal sample is directly controlled by the SSA as it reflects the abundance of adsorption sites for methane molecules. Compared with the SSA, total PV

Table 3: Calculated results of fractal dimensions based on HP-MIP and LP-N_2GA.

Sample	HP-MIP						LP-N_2GA		
	$D > 50$ nm			$D = 3 - 50$ nm			$D = 1 - 50$ nm		
	K_{m1}	D_{m1}	R^2	K_{m2}	D_{m2}	R^2	K_n	D_n	R^2
ZC-S5	-1.18	2.82	0.9719	-0.21	3.79	0.6842	-0.42	2.58	0.9995
ZC-S8	-1.11	2.89	0.9818	-0.17	3.83	0.3823	-0.50	2.50	0.9993
ZC-Q9	-1.19	2.81	0.9728	-0.25	3.75	0.8549	-0.38	2.62	0.9992
ZC-S12	-1.19	2.81	0.9671	-0.29	3.71	0.8841	-0.39	2.61	0.9877
TC-1	-1.10	2.90	0.9772	-0.28	3.72	0.9308	-0.33	2.67	0.9968
TC-2	-1.07	2.93	0.9691	-0.32	3.68	0.4517	-0.36	2.64	0.9984
TC-3	-1.15	2.85	0.9830	-0.29	3.71	0.8876	-0.27	2.73	0.9985
TC-4	-1.03	2.97	0.9699	-0.37	3.63	0.9305	-0.30	2.70	0.9803

Notes: D_{m1} and D_{m2} are the fractal dimensions calculated based on HP-MIP data with pore size greater than 50 nm and 3–50 nm, respectively. D_n is the fractal dimension calculated based on LP-N2GA data with pore size 1–50 nm. K_{m1}, K_{m2}, and K_n are the corresponding fitting parameters.

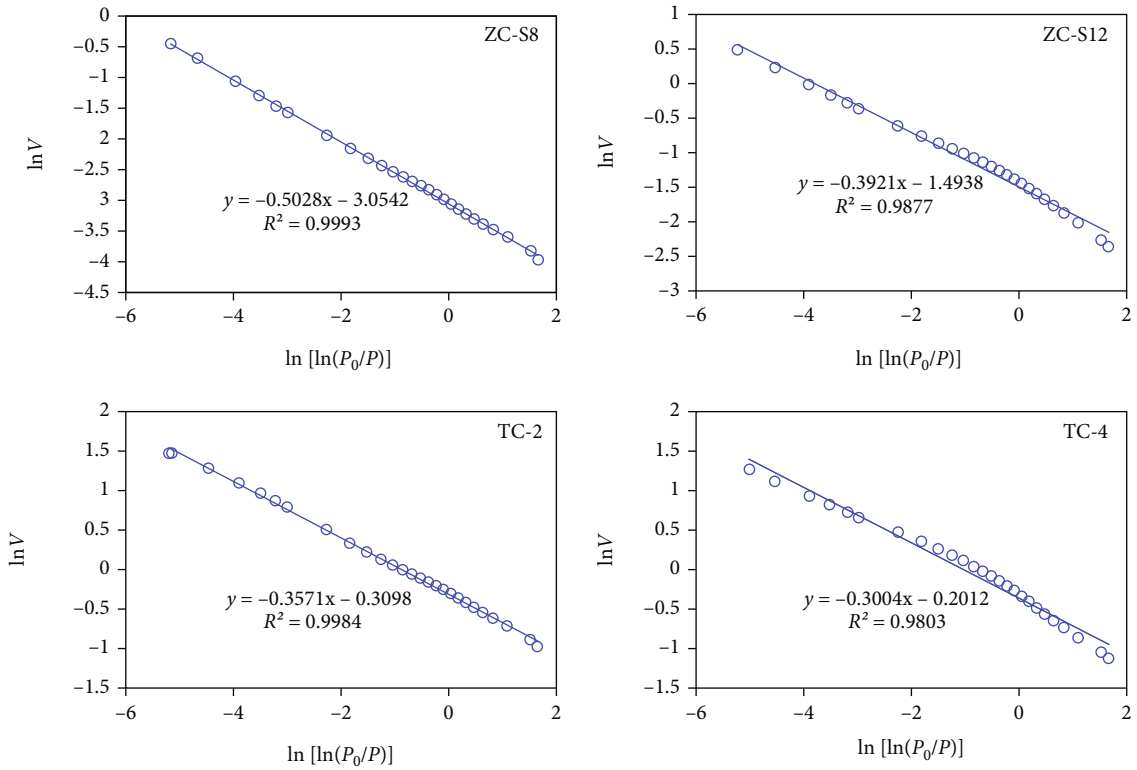

Figure 7: Plots of ln V and ln [ln (P_0/P)] of the representative coal samples based on the LP-N_2GA measurements.

weakly correlates with the V_L, especially for the outburst coal samples with high methane adsorption capacities (Figure 9(a)). Considering the different effects of pores with different sizes on methane adsorption, the correlations between the maximum methane adsorption capacities and the PV of micro-, transition-, meso- and macropores are illustrated in Figure 10. The results show that the maximum methane adsorption capacities exhibit a positive linear correlation with the micropore volume ($R^2 = 0.8757$) and transition pore volume ($R^2 = 0.8386$), respectively (Figure 10(a)), while the data points representing the maximum methane adsorption capacity versus meso- and macro- pore volumes are relatively scattered without obvious correlation (Figure 10(b)).

The pores with different sizes differ in the contribution to the PV and SSA. As shown in Figure 11(a), the total PV of the coal samples is mainly provided by macropores and mesopores. Macropores occupy the largest percentage of the total PV, i.e., 41.4%–59.7% (average: 48.3%), followed by mesopores with the percentage of 19.9%–47.2% (average: 31.3%). However, the total SSA is mainly contributed by micropores and transition pores (Figure 11(b)). The micropores dominated the total SSA with the percentage of 37.3%–82.0% (average: 67.2%), followed by transition pores with the percentage of 13.5%–53.3% (average: 26.6%). On the one hand, given the same total PV, the micro- and transition pores can provide a larger surface area than meso- and

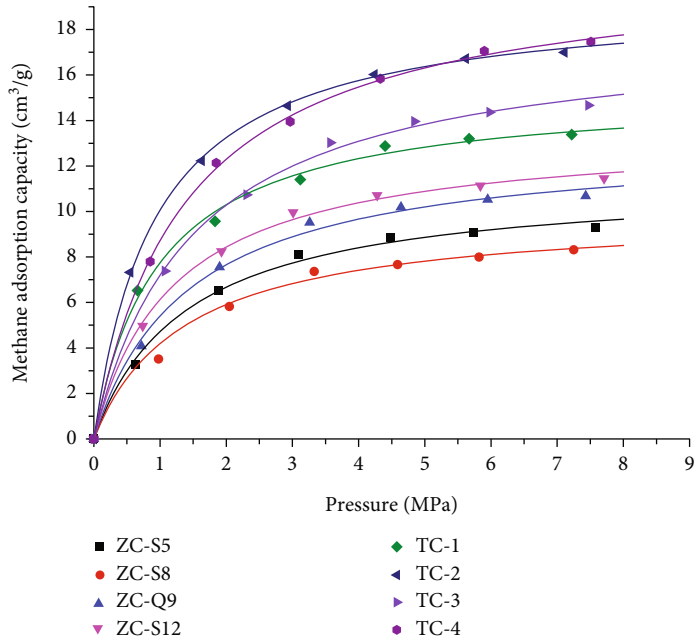

Figure 8: Methane adsorption isotherms of the coal samples.

Table 4: Fitting results of adsorption parameters for the coal samples.

Sample	V_L (cm^3/g)	P_L (MPa)	R^2
ZC-S5	11.35	1.40	0.9965
ZC-S8	9.97	1.38	0.9976
ZC-Q9	13.10	1.42	0.9962
ZC-S12	13.51	1.20	0.9980
TC-1	15.34	0.98	0.9965
TC-2	19.43	0.93	0.9997
TC-3	17.99	1.50	0.9981
TC-4	20.86	1.39	0.9992

macropores for methane adsorption. On the other hand, the distance is relatively short between the pore walls in micro- and transition pores. It may cause the van der Waals force field to overlap between the pore walls, resulting in the larger adsorption potential in nanopores [16, 55]. Therefore, micropores and transition pores are the governing factors on gas adsorption capacity in coal seams. The well-developed micro- and transition pores in the outburst coal are accompanied by a rich internal surface, which enhances the gas adsorption capacity and expansion potentiality.

4.2. Effect of Fractal Dimension on Methane Adsorption Capacity. The complexity of the pore structure is another key factor affecting the gas adsorption capacity [13, 35, 42, 56]. Even if coal samples have the same PV or SSA, the pore complexity may be completely different, which is expressed by fractal dimensions D_n ($D < 50$ nm) and D_{m1} ($D > 50$ nm) in this study. It can be seen from Figure 12 that the V_L presents a positive relationship with D_n ($R^2 = 0.6969$), as the maximum methane adsorption capacity increases with the increasing D_n of the coal samples. However, the correlation is unobvious between the maximum adsorption capacity and D_{m1}. The physical meanings represented by D_n and D_{m1} are different. The D_n was calculated based on the N_2 adsorption branch and FHH model, and D_{m1} was obtained according to the mercury intrusion branch and Menger model. As LP-N_2GA measurement mainly indicates the interaction between nitrogen molecules and the pore surface of coal matrix [54], D_n describes the complexity and roughness of the pore surface. Nevertheless, the HP-MIP experiment is a process that the mercury fluid flows through the pore throat and injects into the pore body via pressure elevation [27, 28]; thus, D_{m1} reflects the complexity and irregularity of the spatial structure. Therefore, fractal dimension D_n of the pore surface is closely related to gas adsorption capacities, whereas fractal dimension D_{m1} of the pore spatial structure presents an unobvious effect on gas adsorptivity.

We further analyze the effect of the fractal dimension on the methane adsorption capacities by plotting the D_n and total SSA of the coal samples (Figure 13). The results show that the total SSA presents a positive correlation with D_n, which also proves that the D_n mainly reflects the complexity and roughness of the pore surface. The coal sample with a higher D_n value possesses a larger specific surface area, thereby facilitating the methane adsorption capacity.

4.3. Fractal Pore Structure of Outburst Coal and Its Geological Significance

4.3.1. Comparison of Fractal Pore Characteristics between Outburst and Nonoutburst Coals. The pore structure and fractal heterogeneity of the coal reservoir are closely related to the gas occurrence since they affect the methane adsorption capacities of the coal samples. The differences of pore structure (including porosity, PV, SSA, PSD, and pore

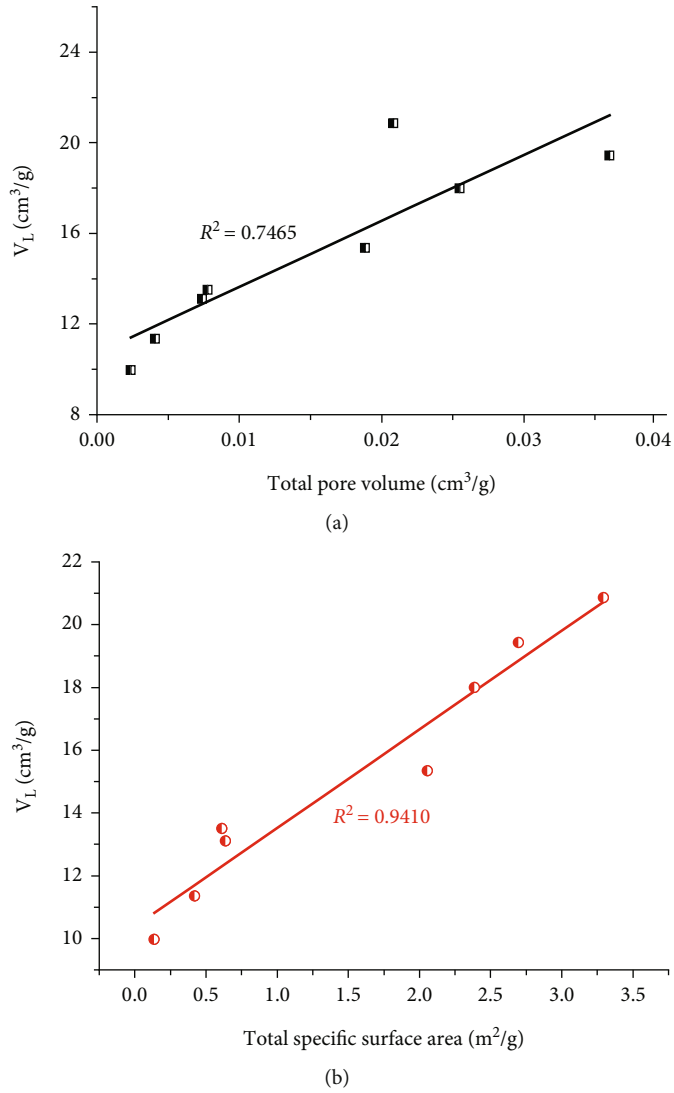

Figure 9: Correlations between the maximum methane adsorption capacity and total pore volume (a) and total specific surface area (b).

shape) and fractal characteristics between the outburst coal and nonoutburst coal were compared, and their geological significance was analyzed. The porosity, PV, and SSA of the outburst coal samples vary from 4.69% to 7.29%, 0.0188–0.0360 cm^3/g, and 2.388–3.294 m^2/g, respectively (Table 2). The porosity, PV, and SSA of the nonoutburst coal samples are 2.24%–3.98%, 0.0024–0.0078 cm^3/g, and 0.139–0.640 m^2/g, respectively. Compared to the nonoutburst coal samples, the porosity, PV, and SSA of outburst coal samples are significantly higher (Figure 11). Quantitatively, the porosity, PV, and SSA of the outburst coal are 1.82 times, 4.56 times, and 5.77 times those of the nonoutburst coal on average, respectively. The well-developed porosity of the outburst coal has two aspects of geological significance to coalbed gas occurrence and outburst. On the one hand, the larger PV leads to the thinner coal skeleton in unit volume, and thus, the coal body is characterized by low strength and fragile structure. On the other hand, the rich surface area inside the outburst coal provides sufficient adsorption sites for methane molecules, and the large pore volume provides sufficient space for gas storage. Therefore, gas is easy to accumulate in the outburst coal seam, which increases gas pressure and outburst tendency.

The pore shape of coal can be analyzed based on the hysteresis loops determined by the mercury intrusion/extrusion and the N_2 adsorption/desorption [35, 54]. Yao and Liu [57] concluded that the open pore and inkbottle pore can retain mercury and lead to a hysteresis loop, while the semiclosed pore cannot. Taking samples ZC-S8 and TC-4 as an example, the difference of pore shape between the outburst coal and nonoutburst coal can be analyzed. As shown in Figure 14(a), the hysteresis loops of the nonoutburst coal are narrow or inconspicuous. Accordingly, the nonoutburst coal is dominated by semiclosed pores, including narrow slit-like pores, wedge-shaped pores, and conical/tubular pores with a closed end. This type of pore system is of poor openness and connectivity, which is not conducive to gas occurrence and enrichment. However, the hysteresis loops of the outburst coal are wide, and the N_2 desorption branch presents a sharp decline (Figure 14(b)). Therefore, the pores

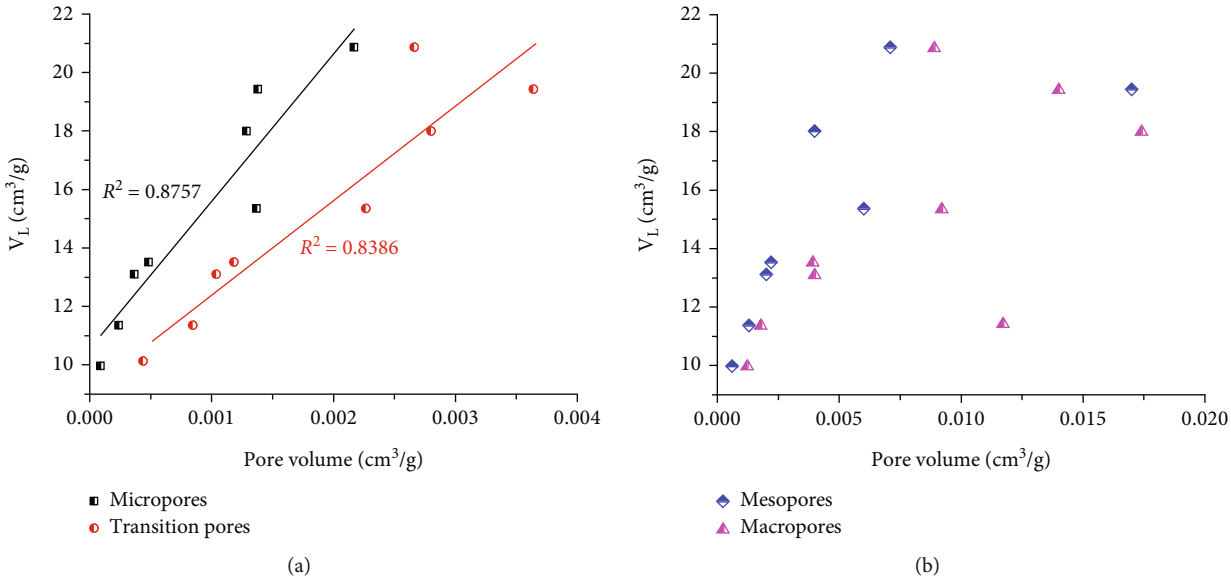

Figure 10: Correlations between the maximum methane adsorption capacity and pore volume of micro- and transition pores (a) and meso- and macropores (b).

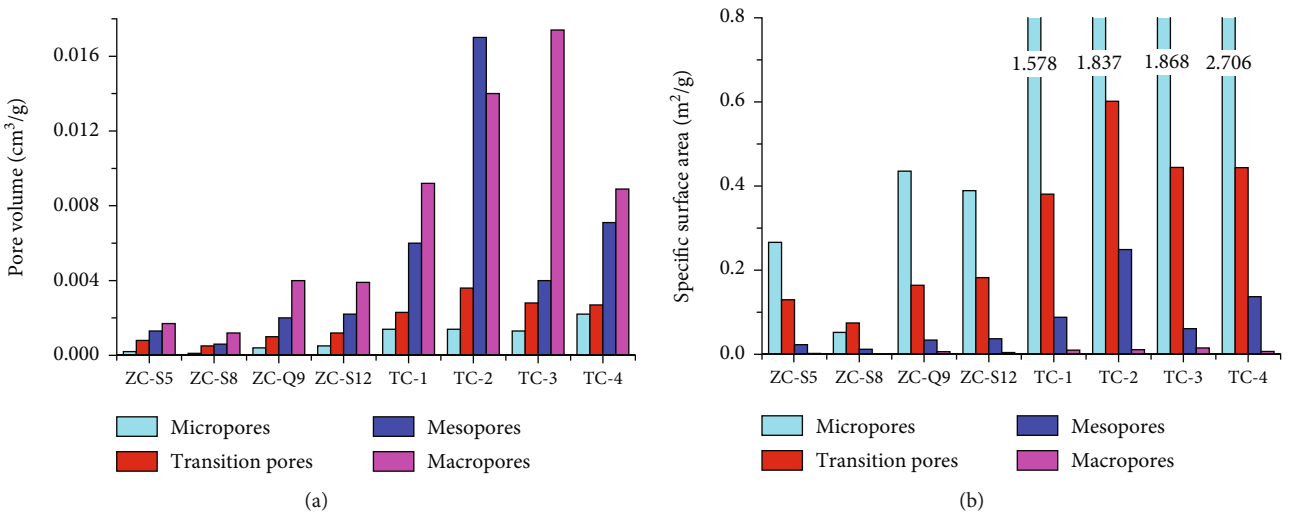

Figure 11: Pore volume (a) and specific surface area (b) distributions for different pore sizes in the coal samples.

in the outburst coal are mainly open pores, including parallel plate-like pores open on all sides and cylindrical pores open at both ends. In addition, there are a certain number of inkbottle pores with narrow throats and wide bodies, which limit the pore connectivity. This type of pore structure is beneficial to gas enrichment and storage, and abundant gas can be stored in the wide bottle body of the inkbottle pores. More importantly, the narrow pore throat restricts the gas seepage. Thus, the gas does not migrate but accumulates locally to form a high-pressure gas zone.

PSD is directly related to the occurrence and migration of coalbed gas. Micro- and transition pores provide the primary space for adsorbed gas, while meso- and macropores mainly constitute the diffusion and seepage space for free gas [15, 28]. LP-N_2GA and HP-MIP were combined to characterize PSD in pore sizes ranging from 1 to 50 nm and >50 nm, respectively, according to their advantages. As the full-scale PSDs are shown in Figure 15, the nonoutburst coal is dominated by micropores. However, the pore size is widely distributed in the outburst coal, in which not only micropores are dominant, but also, transition pores and mesopores are developed to a certain extent. The difference of PSDs between outburst and nonoutburst coals is mainly affected by tectonic deformation. As the degree of tectonic deformation increases (sequence from primary coal, cataclastic coal, scaly coal, to wrinkle coal), the micropores in TDC increase significantly because of the squeezing action [12], which corresponds to the narrow throat of the inkbottle pores in the outburst coal. In addition, new macropores and microfractures were formed in TDC under the tectonic deformation, which provides a favorable channel for rapid and instantaneous gas release in gas outburst.

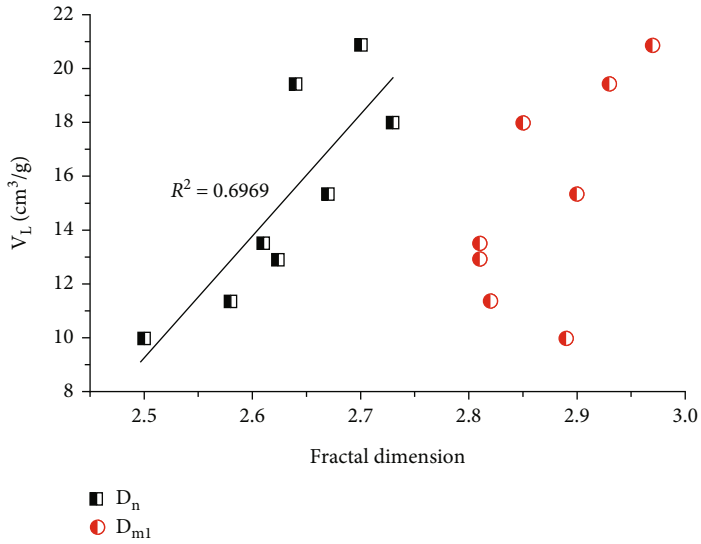

Figure 12: Relationship between the maximum methane adsorption capacity and fractal dimensions.

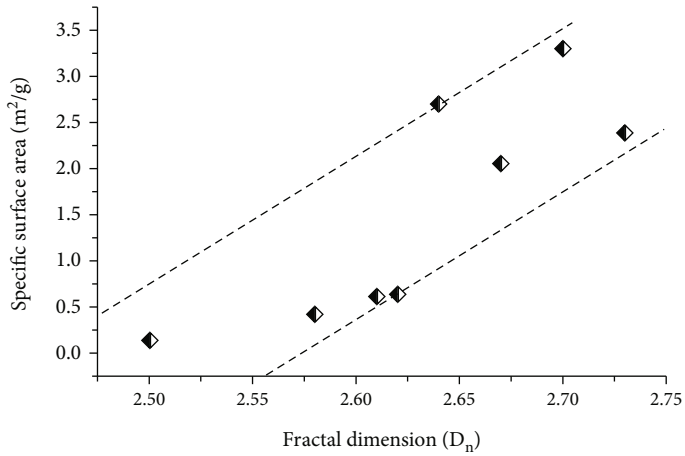

Figure 13: Relationship between total specific surface areas and fractal dimension D_n.

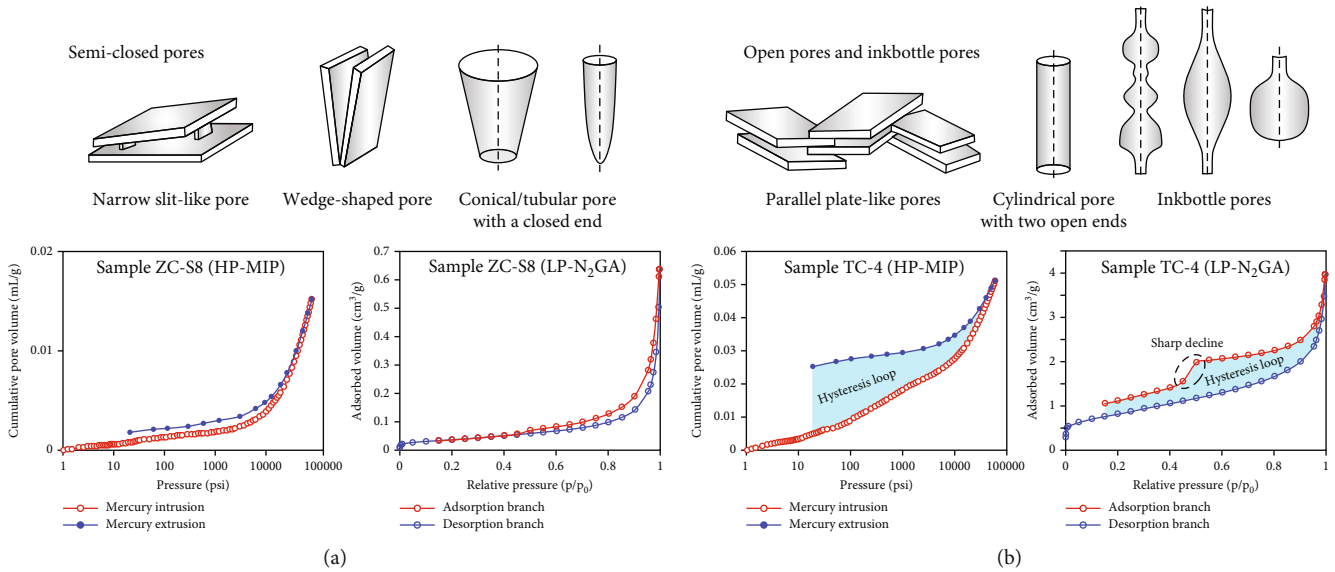

Figure 14: Schematic diagram of pore shape for the nonoutburst coal (a) and outburst coal (b) based on the HP-MIP and LP-N_2GA data.

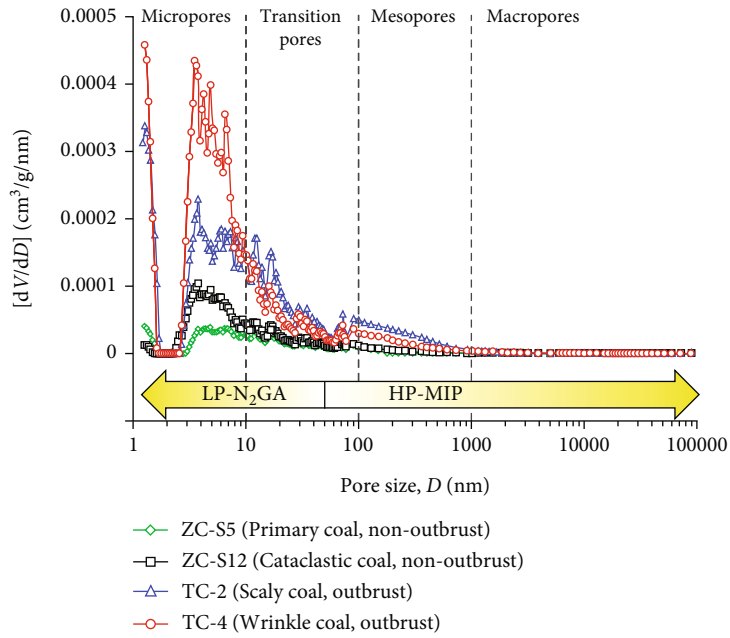

Figure 15: The pore size distribution of the coal samples from HP-MIP and LP-N_2GA data.

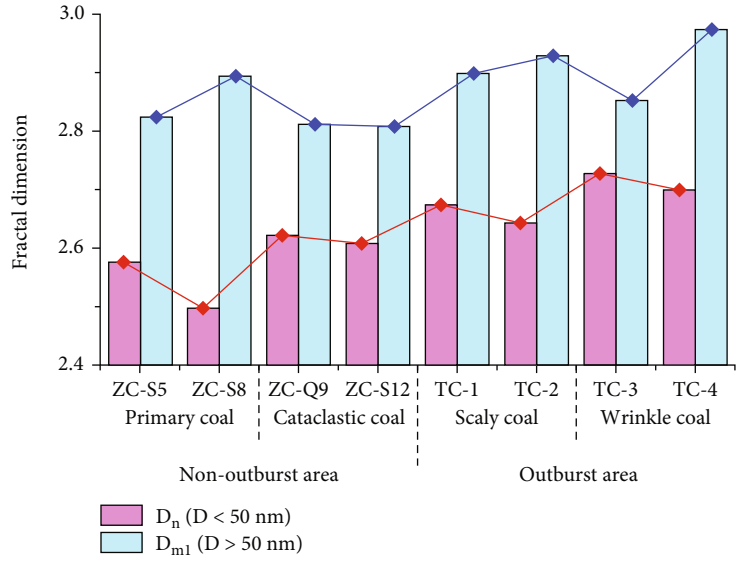

Figure 16: Fractal dimensions of the coal samples with different tectonically deformed types.

According to the comparison of the fractal dimensions between the nonoutburst coal and outburst coal (Figure 16), D_n and D_{m1} of the nonoutburst coal samples vary from 2.50 to 2.62 (2.58 on average) and 2.81–2.89 (2.83 on average), respectively, while D_n and D_{m1} of the outburst coal samples range within 2.64–2.73 (2.69 on average) and 2.85–2.97 (2.91 on average), respectively. Both D_n and D_{m1} of the outburst coal are generally larger than those of the nonoutburst coal, which suggests that the pore structure in the outburst coal is more complex and heterogeneous. Additionally, with the increase of the degree of tectonic deformation, D_n shows an increasing trend (Figure 16), while the changing trend is less evident for D_{m1}. Therefore, the fractal heterogeneity of pores below 50 nm is more sensitive to tectonic deformation than that of pores above 50 nm.

4.3.2. Geological Implication of Fractal Pore Structure on Gas Occurrence and Outburst. The coal and gas outburst occurred in the zone of TDC including scaly coal and wrinkle coal in the study area. Meanwhile, there are significant differences in pore structure between TDC and primary coal as mentioned in Section 4.3.1. To reveal the relationship between tectonic deformation and gas outburst, the combined effect of tectonic deformation, pore structure, and adsorption capacity of coal reservoir on gas occurrence and outburst was summarized. Under the tectonic deformation,

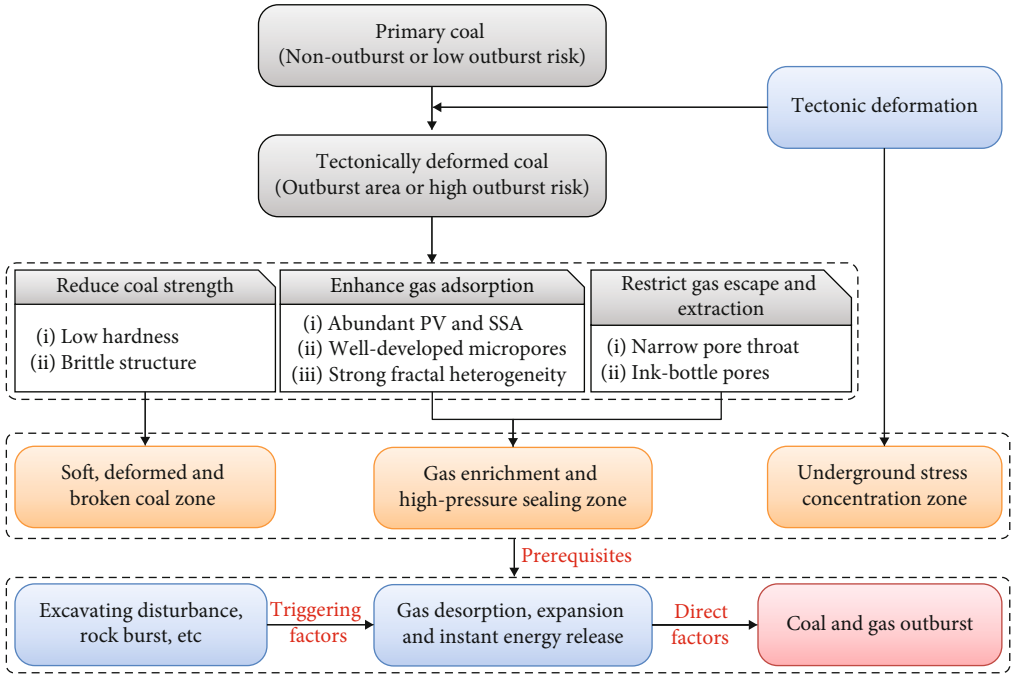

Figure 17: The combined effect of tectonic deformation, pore structure, and gas adsorptivity on coalbed gas occurrence and outburst.

the primary coal transits to TDC accompanied by the direct effect on the physical properties and pore structure (Figure 17). Firstly, the coal strength is reduced yielding low hardness and brittle structure, thus forming the zone of soft and broken coal. Secondly, TDC is characterized by abundant PV and SSA and developed microporosity and strong fractal heterogeneity, resulting in a large number of internal surfaces for methane adsorption. Accordingly, the gas adsorption capacities of TDCs are remarkably enhanced. Thirdly, inkbottle pores with narrow throats emerge under the tectonic deformation, resulting in poor pore connectivity, which is unfavorable for gas migration and extraction. In addition, the TDC area is also a geostress concentration zone with high stress and high energy. Cheng and Lei [58] also suggested that in situ coal reservoirs in the TDC area possess low permeability as the fracture system was severely squeezed. Therefore, TDC is of strong adsorption capacity but poor permeability, and coalbed gas is enriched to form a high-pressure gas sealing zone.

In fact, coal and gas outburst can be regarded as a combined action of gas, the porous medium of coal/rock, and underground stress according to the integrated factor outburst hypothesis [11]. Li [59] proposed that, for coal and gas outburst, high-pressure gas is an essential factor, while coal structure is an obstacle, and underground stress acts as a dynamic factor. The place, where TDC is well-developed, is in an unstable state due to the combination of soft and deformed coal zone, high-pressure gas sealing zone, and underground stress concentration zone (Figure 17). Once the triggering factors (excavating disturbance, rock burst, active geological structure, temperature anomaly, etc.) break the original equilibrium state, the adsorbed gas is desorbed to free gas rapidly, resulting in a gas expansion in the coal reservoir. Ultimately, high-pressure free gas and crushed coal powder/block are released instantaneously driven by stress energy, which leads to abnormal gas emission, even continuous coal fragmentation, and gas outburst. In summary, weak coal structure, abundant gas enrichment, and concentrating underground stress are the prerequisites for coal and gas outburst. The risk of gas outburst in the zone of TDC is higher than that in the zone of primary coal.

5. Conclusions

In this work, qualitative description, quantitative experiments, and fractal dimension calculation have been carried out to compare the pore structure and methane adsorption capacity between outburst and nonoutburst coals. Further, the effects of fractal pore on gas adsorption capacity and its geological significance to coalbed gas occurrence and outburst were discussed. The following conclusions can be drawn from the present study.

(1) On average, the PV and SSA of outburst coal samples are 4.56 and 5.77 times those of nonoutburst coal samples, respectively. The pore size is widely distributed in the outburst coal compared with the nonoutburst coal. Developed porosity in the outburst coal is beneficial to gas enrichment but leads to weak coal strength. Meanwhile, the considerable inkbottle pores in the outburst coal restrict gas migration and extraction, which is an important microscopic factor leading to gas outburst

(2) Pore structure in coal reservoir exhibits fractal characteristics. The fractal dimensions D_n ($D < 50$ nm) and D_{m1} ($D > 50$ nm) can be calculated based on HP-MIP and LP-N_2GA, respectively. The pore structure

of the outburst coal is more complex and heterogeneous as its D_n and D_{m1} values are generally larger than those of the nonoutburst coal. In addition, the D_n is more sensitive to tectonic deformation than D_{m1}

(3) The methane adsorption capacities of the coal samples are governed by micropores and transition pores and affected by the fractal dimension D_n as well. The rich micro- and transition pores and complex pore surface are accompanied by abundant internal surface area, resulting in the significantly stronger gas adsorption capacity of the outburst coal than that of the nonoutburst coal

(4) The outburst coal is mostly scaly coal and wrinkle coal with tectonic deformation in the study area. The TDC is characterized by weak coal strength, complex pore structure, and strong adsorption capacity but limited permeability. Therefore, the area of TDC is at high risk for gas outburst, where there is a combination of soft coal zone, high-pressure gas sealing zone, and underground stress concentration zone

Data Availability

The data used to support the findings of this study are included within the article.

Conflicts of Interest

The authors declare that they have no known competing financial interests or personal relationships that could have appeared to influence the work reported in this paper.

Acknowledgments

This research was jointly supported by the National Natural Science Foundation of China (Grant Nos. 42202190, 42172156, and 42072199); the Natural Science Foundation of Jiangsu Province, China (Grant No. BK20221147); and the Fundamental Research Funds for the Central Universities (Grant No. 2022-11247).

References

[1] C. O. Karacan, F. A. Ruiz, M. Cote, and S. Phipps, "Coal mine methane: a review of capture and utilization practices with benefits to mining safety and to greenhouse gas reduction," *International Journal of Coal Geology*, vol. 86, no. 2-3, pp. 121–156, 2011.

[2] B. Kong, Z. Cao, T. Sun, C. Qi, and Y. Zhang, "Safety hazards in coal mines of Guizhou China during 2011-2020," *Safety Science*, vol. 145, article 105493, 2022.

[3] Y. Li, S. Pan, S. Ning, L. Shao, Z. Jing, and Z. Wang, "Coal measure metallogeny: metallogenic system and implication for resource and environment," *Science China Earth Sciences*, vol. 65, no. 7, pp. 1211–1228, 2022.

[4] Y. Li, J. Yang, Z. Pan, S. Meng, K. Wang, and X. Niu, "Unconventional natural gas accumulations in stacked deposits: a discussion of Upper Paleozoic coal-bearing strata in the east margin of the Ordos Basin, China," *Acta Geologica Sinica-English Edition*, vol. 93, no. 1, pp. 111–129, 2019.

[5] A. Fisne and O. Esen, "Coal and gas outburst hazard in Zonguldak Coal Basin of Turkey, and association with geological parameters," *Natural Hazards*, vol. 74, no. 3, pp. 1363–1390, 2014.

[6] Q. Zhang, C. Yang, X. Li, Z. Li, and Y. Li, "Mechanism and classification of coal and gas outbursts in China," *Advances in Civil Engineering*, vol. 2021, Article ID 5519853, 12 pages, 2021.

[7] L. Hong, D. Gao, J. Wang, and D. Zheng, "A distinguishing method of coal and gas outburst based on the adsorption capacity in pores," *Energy sources. Part A, Recovery, utilization, and environmental effects*, vol. 42, no. 11, pp. 1402–1411, 2020.

[8] D. Yang, L. Pan, Y. Chen, and J. Tang, "Comparison of outburst hazard of coal with different failure types: a case study," *Energy Sources, Part A: Recovery, Utilization, and Environmental Effects*, pp. 1–3, 2021.

[9] Y. Lei, Y. Cheng, T. Ren, Q. Tu, Y. Li, and L. Shu, "Experimental investigation on the mechanism of coal and gas outburst: novel insights on the formation and development of coal spallation," *Rock Mechanics and Rock Engineering*, vol. 54, no. 11, pp. 5807–5825, 2021.

[10] D. Xu and D. Guo, "Dome-basin structure and its influence on coal and gas outbursts," *Polish Journal of Environmental Studies*, vol. 27, no. 4, pp. 1823–1831, 2018.

[11] K. Zhang, L. Wang, Y. Cheng et al., "Geological control of fold structure on gas occurrence and its implication for coalbed gas outburst: case study in the Qinan coal mine, Huaibei coalfield, China," *Natural Resources Research*, vol. 29, no. 2, pp. 1375–1395, 2020.

[12] Y. Song, B. Jiang, M. Li, C. Hou, and S. Xu, "A review on pore-fractures in tectonically deformed coals," *Fuel*, vol. 278, article 118248, 2020.

[13] Y. Cai, D. Liu, Z. Pan, Y. Yao, J. Li, and Y. Qiu, "Pore structure and its impact on CH_4 adsorption capacity and flow capability of bituminous and subbituminous coals from Northeast China," *Fuel*, vol. 103, pp. 258–268, 2013.

[14] C. R. Clarkson, N. Solano, R. M. Bustin et al., "Pore structure characterization of North American shale gas reservoirs using USANS/SANS, gas adsorption, and mercury intrusion," *Fuel*, vol. 103, no. 1, pp. 606–616, 2013.

[15] Y. Yao, D. Liu, D. Tang, S. Tang, and W. Huang, "Fractal characterization of adsorption-pores of coals from North China: an investigation on CH_4 adsorption capacity of coals," *International Journal of Coal Geology*, vol. 73, no. 1, pp. 27–42, 2008.

[16] Y. Song, B. Jiang, and J. Liu, "Nanopore structural characteristics and their impact on methane adsorption and diffusion in low to medium tectonically deformed coals: case study in the Huaibei coal field," *Energy & Fuels*, vol. 31, no. 7, pp. 6711–6723, 2017.

[17] Y. Li, Z. Wang, S. Tang, and D. Elsworth, "Re-evaluating adsorbed and free methane content in coal and its ad- and desorption processes analysis," *Chemical Engineering Journal*, vol. 428, article 131946, 2022.

[18] Y. Li, J. Yang, Z. Pan, and W. Tong, "Nanoscale pore structure and mechanical property analysis of coal: an insight combining AFM and SEM images," *Fuel*, vol. 260, article 116352, 2020.

[19] Y. Li, C. Zhang, D. Tang et al., "Coal pore size distributions controlled by the coalification process: an experimental study of coals from the Junggar, Ordos and Qinshui basins in China," *Fuel*, vol. 206, pp. 352–363, 2017.

[20] G. Feng, Y. Zhu, S. Chen et al., "Supercritical methane adsorption on shale over wide pressure and temperature ranges: implications for gas-in-place estimation," *Energy & Fuels*, vol. 34, no. 3, pp. 3121–3134, 2020.

[21] L. Si, H. Zhang, J. Wei, B. Li, and H. Han, "Modeling and experiment for effective diffusion coefficient of gas in water-saturated coal," *Fuel*, vol. 284, article 118887, 2021.

[22] Y. Ma, M. Wang, R. Ma, J. Li, A. Bake, and Y. Shan, "Micropore characteristics and gas-bearing characteristics of marine-continental transitional shale reservoirs in the east margin of Ordos Basin," *Adsorption Science & Technology*, vol. 2021, article 5593245, pp. 1–15, 2021.

[23] Z. Zhang, Y. Qin, G. Wang et al., "Evaluation of coal body structures and their distributions by geophysical logging methods: case study in the Laochang block, eastern Yunnan, China," *Natural Resources Research*, vol. 30, no. 3, pp. 2225–2239, 2021.

[24] J. Zheng, H. Liu, K. Wang, and Z. You, "A new capillary pressure model for fractal porous media using percolation theory," *Journal of Natural Gas Science and Engineering*, vol. 41, pp. 7–16, 2017.

[25] B. B. Hodot, *Outburst of Coal and Coalbed Gas (Chinese Translation)*, China Coal Industry Press, Beijing, 1966.

[26] S. Giffin, R. Littke, J. Klaver, and J. L. Urai, "Application of BIB-SEM technology to characterize macropore morphology in coal," *International Journal of Coal Geology*, vol. 114, pp. 85–95, 2013.

[27] Z. Spitzer, "Mercury porosimetry and its application to the analysis of coal pore structure," *Powder Technology*, vol. 29, no. 1, pp. 177–186, 1981.

[28] Y. Yao, D. Liu, D. Tang et al., "Fractal characterization of seepage-pores of coals from China: an investigation on permeability of coals," *Computers & Geosciences*, vol. 35, no. 6, pp. 1159–1166, 2009.

[29] Y. Bao, Y. Ju, Z. Yin, J. Xiong, G. Wang, and Y. Qi, "Influence of reservoir properties on the methane adsorption capacity and fractal features of coal and shale in the upper Permian coal measures of the South Sichuan coalfield, China," *Energy Exploration & Exploitation*, vol. 38, no. 1, pp. 57–78, 2020.

[30] A. P. Radlinski, M. Mastalerz, A. L. Hinde et al., "Application of SAXS and SANS in evaluation of porosity, pore size distribution and surface area of coal," *International Journal of Coal Geology*, vol. 59, no. 3-4, pp. 245–271, 2004.

[31] M. Mastalerz, L. He, Y. B. Melnichenko, and J. A. Rupp, "Porosity of coal and shale: insights from gas adsorption and SANS/USANS techniques," *Energy & Fuels*, vol. 26, no. 8, pp. 5109–5120, 2012.

[32] B. Sun, Q. Yang, J. Zhu et al., "Pore size distributions and pore multifractal characteristics of medium and low-rank coals," *Scientific Reports*, vol. 10, no. 1, article 22353, 2020.

[33] M. Zhang, X. Fu, C. Duan, and Y. Li, "Influencing factor analysis of the coal matrix compressibility of middle-high rank coals," *Journal of Natural Gas Science and Engineering*, vol. 81, article 103462, 2020.

[34] X. Liu, X. Kong, B. Nie, D. Song, X. He, and L. Wang, "Pore fractal dimensions of bituminous coal reservoirs in North China and their impact on gas adsorption capacity," *Natural Resources Research*, vol. 30, no. 6, pp. 4585–4596, 2021.

[35] G. Feng, Y. Zhu, G. G. X. Wang, S. Chen, Y. Wang, and W. Ju, "Supercritical methane adsorption on overmature shale: effect of pore structure and fractal characteristics," *Energy & Fuels*, vol. 33, no. 9, pp. 8323–8337, 2019.

[36] Y. Qin, T. A. Moore, J. Shen, Z. Yang, Y. Shen, and G. Wang, "Resources and geology of coalbed methane in China: a review," *International Geology Review*, vol. 60, no. 5-6, pp. 777–812, 2018.

[37] S. Lu, Y. Zhang, Z. Sa, and S. Si, "Evaluation of the effect of adsorbed gas and free gas on mechanical properties of coal," *Environmental Earth Sciences*, vol. 78, no. 6, 2019.

[38] J. Bae and S. K. Bhatia, "High-pressure adsorption of methane and carbon dioxide on coal," *Energy & Fuels*, vol. 20, no. 6, pp. 2599–2607, 2006.

[39] P. J. Crosdale, T. A. Moore, and T. E. Mares, "Influence of moisture content and temperature on methane adsorption isotherm analysis for coals from a low-rank, biogenically-sourced gas reservoir," *International Journal of Coal Geology*, vol. 76, no. 1-2, pp. 166–174, 2008.

[40] B. V. Krooss, F. Van Bergen, Y. Gensterblum, N. Siemons, H. Pagnier, and P. David, "High-pressure methane and carbon dioxide adsorption on dry and moisture- equilibrated Pennsylvanian coals," *International Journal of Coal Geology*, vol. 51, no. 2, pp. 69–92, 2002.

[41] C. R. Clarkson and R. M. Bustin, "Binary gas adsorption/desorption isotherms: effect of moisture and coal composition upon carbon dioxide selectivity over methane," *International Journal of Coal Geology*, vol. 42, no. 4, pp. 241–271, 2000.

[42] L. Chen, Z. Jiang, K. Liu, W. Yang, S. Jiang, and J. Tan, "Investigation of fractal characteristics and methane adsorption capacity of the Upper Triassic lacustrine shale in the Sichuan Basin, southwest China," *Fractals*, vol. 27, no. 1, article 1940011, 2019.

[43] Q. Tu, Y. Cheng, T. Ren, Z. Wang, J. Lin, and Y. Lei, "Role of tectonic coal in coal and gas outburst behavior during coal mining," *Rock Mechanics and Rock Engineering*, vol. 52, no. 11, pp. 4619–4635, 2019.

[44] W. Li, B. Jiang, and Y. Zhu, "Impact of tectonic deformation on coal methane adsorption capacity," *Adsorption Science & Technology*, vol. 37, no. 9-10, pp. 698–708, 2019.

[45] E. W. Washburn, "The dynamics of capillary flow," *Physical Review*, vol. 17, no. 3, pp. 273–283, 1921.

[46] E. P. Barrett, L. G. Joyner, and P. P. Halenda, "The determination of pore volume and area distributions in porous substances. I. Computations from nitrogen isotherms," *Journal of the American Chemical Society*, vol. 73, no. 1, pp. 373–380, 1951.

[47] S. Brunauer, P. H. Emmett, and E. Teller, "Adsorption of gases in multimolecular layers," *Journal of the American Chemical Society*, vol. 60, no. 2, pp. 309–319, 1938.

[48] K. S. W. Sing, D. H. Everett, R. A. W. Haul et al., "Reporting physisorption data for gas/solid systems with special reference to the determination of surface area and porosity (recommendations 1984)," *Pure and Applied Chemistry*, vol. 57, no. 4, pp. 603–619, 1985.

[49] G. R. Chalmers, R. M. Bustin, and I. M. Power, "Characterization of gas shale pore systems by porosimetry, pycnometry, surface area, and field emission scanning electron microscopy/transmission electron microscopy image analyses: examples

from the Barnett, Woodford, Haynesville, Marcellus, and Doig units," *AAPG Bulletin*, vol. 96, no. 6, pp. 1099–1119, 2012.

[50] M. Mastalerz, A. Schimmelmann, A. Drobniak, and Y. Chen, "Porosity of Devonian and Mississippian New Albany Shale across a maturation gradient: insights from organic petrology, gas adsorption, and mercury intrusion," *AAPG Bulletin*, vol. 97, no. 10, pp. 1621–1643, 2013.

[51] I. Langmuir, "The adsorption of gases on plane surfaces of glass, mica and platinum," *Journal of the American Chemical Society*, vol. 40, no. 9, pp. 1361–1403, 1918.

[52] D. Avnir and M. Jaroniec, "An isotherm equation for adsorption on fractal surfaces of heterogeneous porous materials," *Langmuir*, vol. 5, no. 6, pp. 1431–1433, 1989.

[53] P. Pfeiferper and D. Avnir, "Chemistry nonintegral dimensions between two and three," *The Journal of Chemical Physics*, vol. 79, no. 7, pp. 3369–3558, 1983.

[54] M. Thommes, K. Kaneko, A. V. Neimark et al., "Physisorption of gases, with special reference to the evaluation of surface area and pore size distribution (IUPAC technical report)," *Pure and Applied Chemistry*, vol. 87, no. 9-10, pp. 1051–1069, 2015.

[55] K. Mosher, J. He, Y. Liu, E. Rupp, and J. Wilcox, "Molecular simulation of methane adsorption in micro- and mesoporous carbons with applications to coal and gas shale systems," *International Journal of Coal Geology*, vol. 109-110, pp. 36–44, 2013.

[56] Y. Liu, Y. Zhu, Y. Wang, and S. Chen, "Fractal characteristics of nanoscale pores in shale and its implications on methane adsorption capacity," *Fractals*, vol. 27, no. 1, article 1940014, 2019.

[57] Y. Yao and D. Liu, "Effects of igneous intrusions on coal petrology, pore-fracture and coalbed methane characteristics in Hongyang, Handan and Huaibei coalfields, North China," *International Journal of Coal Geology*, vol. 96, pp. 72–81, 2012.

[58] Y. Cheng and Y. Lei, "Causality between tectonic coal and coal and gas outbursts," *Journal of China Coal Society*, vol. 46, no. 1, pp. 180–198, 2021.

[59] H. Li, "Major and minor structural features of a bedding shear zone along a coal seam and related gas outburst, Pingdingshan coalfield, northern China," *International Journal of Coal Geology*, vol. 47, no. 2, pp. 101–113, 2001.